Results of ITER DMS Pellet Material (Neon) Injection into Large Helical Device*)

Akinobu MATSUYAMA and Ryuichi SAKAMOTO[1)]

National Institutes for Quantum Science and Technology, Aomori 039-3212, Japan
[1)]*National Institute for Fusion Science, 322-6 Oroshi-cho, Toki 509-5292, Japan*

(Received 15 December 2021 / Accepted 17 February 2022)

Cryogenic neon pellets of 3 mm in diameter were injected into neutral beam injection (NBI) heated discharges on the Large Helical Device (LHD). The time response of far infrared (FIR) interferometer has pointed out a relatively slow assimilation of the ablated materials compared to the cases of hydrogen injection. This is consistent with the neutral gas and plasma shielding (NGPS) model prediction, showing that strong line emission inside the ablation cloud limits the cloud temperature and the expansion velocity along the magnetic field line. Measured penetration depths were also compared, being well reproduced by the code prediction when the contribution from 180 keV fast ions produced by tangential NBI is taken into account.

Keywords: pellet injection, disruption mitigation, ablation, ITER, Large Helical Device

DOI: 10.1585/pfr.17.2402017

1. Introduction

The Disruption Mitigation System (DMS) is a key plant system to ensure reliable mitigation of thermal and electromagnetic loads due to disruptions in ITER. The presently planned strategy is the injection of solid neon and hydrogen by means of Shattered Pellet Injection (SPI) [1]. However, the experimental data of neon pellet ablation has not been obtained with the same quantity and quality to those for hydrogen isotope pellets. One of the obstacles is injecting a large-size impurity pellet into tokamak plasmas often triggers macroscopic instabilities. The magnetic configuration is distorted disruptively on the timescale even much faster than the pellet assimilation, which is not suitable for detailed measurements of the ablation and assimilation processes of the injected materials.

To fill this gap, the Large Helical Device (LHD) offers a good experimental capability. The size of individual fragments delivered with SPI [2] is sub-mm to mm size, and the largest one is comparable to those used for fueling in the LHD. The injection of such a large solid neon triggers radiation collapse of keV plasmas due to power imbalance. Contrary to the tokamak experiment, nevertheless, because the magnetic configuration of the LHD is sustained by the external coils, it is guaranteed not being distorted by the pellet, which greatly simplifies our interpretation to identify the penetration depths and the post-injection plasma parameters. This paper reports results of the injection of neon pellets into neutral beam injection (NBI) heated discharges during the campaign carried out in 2019-2020.

author's e-mail: matsuyama.akinobu@qst.go.jp

*) This article is based on the presentation at the 30th International Toki Conference on Plasma and Fusion Research (ITC30).

2. Results of Neon Pellet Injection

Because cyrogenic properties of neon are similar to those of hydrogen isotope, the neon injection has become possible with the replacement of the gas in the existing pellet injection system on the LHD. Twenty barrel *in situ* pipe gun injector [3] was used with cylindrical pellets of 3 mm diameter and length, corresponding to $N_p \sim 0.84 \times 10^{21}$ atoms per pellet (where the solid density of neon is about 4×10^{28} m^{-3}). Helium gas at 5 MPa is used as the propellant. The measured velocity $\simeq$ 550 m/s is about a half of the nominal injection velocity of hydrogen pellets, which corresponds to 70% of the value obtained from the ideal gun theory [4]. Although it is generally not easy to launch solid pure neon with the pipe-gun injector without a mechanical punch, raising the temperature of cooling head just before the injection was helpful for the pellet release without broken. Actual temperature near the pellet is unknown but the temperature of the cryogenic heat sink (see Fig. 3 (b) of [3]) was raised up to 19 K ($\pm$ 1 K) from that for the pellet production ($\sim$ 9 K). Although shadowgraphs to check the pellet integrity were not available in the present experiments, the light gate signal that suggested fractures of the pellet was not observed. To observe the emission from the ablated material, we applied a photodiode with a Balmer α filter (656.28 nm; FWHM = 10 nm) routinely used for hydrogen pellets, where Ne-I emission with a wavelength of 659.89 nm is expected to be a dominant line.

Eight discharges sustained by 3.7 - 10 MW tangential NBI heating (whose beam energies were 150 - 180 keV) were used for target plasmas. Two of them (158159 and 158161) were deuterium discharges and the others were hydrogen ones. A typical time history of the experiments is as follows. For discharge 158161, the pellet was in-

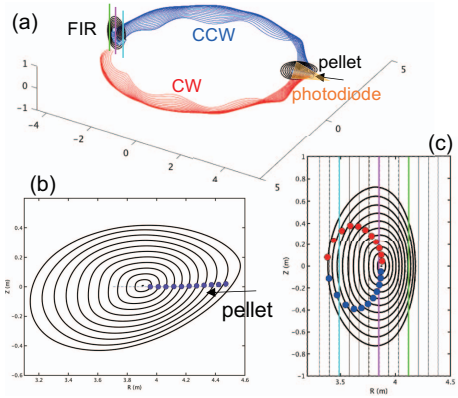

Fig. 1 (a) Top view of the LHD magnetic configuration with the pellet injection and diagnostic ports. (b) The initial points placed along the pellet injection path for the field line tracing. (b) The poloidal cross section and three far infrared (FIR) interferometer chords at $R = 3.489$ m (cyan), 3.849 m (magenta), and 4.029 m (green). The red and blue points are connected to the purple ones in (b) with the magnetic field line traced from the clockwise (CW) and counter-clockwise directions, respectively.

jected at 4004.8 ms at $V_p = 552$ m/s from the outboard side of the torus. The initiation of ablation emission indicates the pellet arrival at the plasma periphery around 4016.6 ms and the emission continued until 4017.5 ms. The penetration depth is estimated to be 45.7 cm if one assumes that the pellet travels at the constant velocity. Associated with the neon injection, a half of the plasma stored energy from 100 kJ to 55.4 kJ was lost within 1.9 ms after the ablation emission ends. This is correlated to a steep rise of the total radiated power observed by the resistive bolometer at the same toroidal location with the pellet injector. We found that the above discharge sequence was in common for the 8-pellet data obtained here.

Figure 1 shows a top view of the experimental layout. Once a radiation collapse is triggered by the pellet, the measurement of plasma density and temperature becomes uneasy but we found that a time margin about 1 - 2 ms before the collapse can be used to measure the ablation emission and initial density increase. Here we utilize the line-integrated density measurement by far infrared (FIR) interferometer at the toroidal location about 180 degree apart from the pellet injection port. Since the ablation emission is measured by the photodiode at the pellet injection port, the time delay from the ablation emission to the density rise involves the information of transport timescale that the ablated materials homogenize over the different toroidal location from the ablation position. If we start the field line tracing from the points placed along the pellet injection path as in Fig. 1 (b), they reach the red and blue points at the inboard side of the poloidal cross section in Fig. 1 (c) from both sides of the toroidal circulation in the clockwise (CW) and counter-clockwise (CCW) direction. The length of the field lines connecting between the two cross sections is about 11 m.

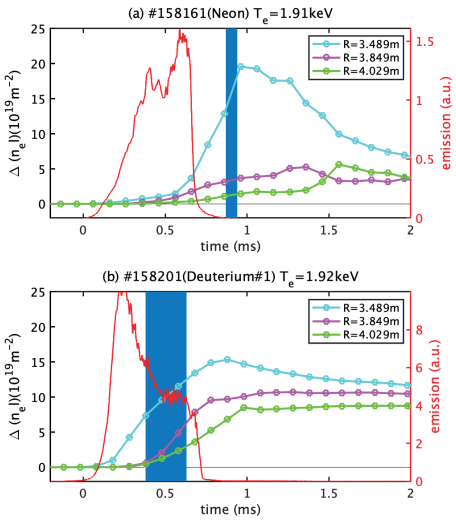

Fig. 2 Time histories of ablation emission and line-integrated electron density increase $\Delta(n_e l)(t) = (n_e l)(t) - (n_e l)(t = 0)$ measured by the FIR interferometer chord of Fig. 1 (c), where $t = 0$ is defined at the beginning of the ablation emission. (a) Neon injection. (b) Deuterium injection. The filled time intervals are NGPS code predictions for the expected arrival time of ablation clouds to the toroidal location of the FIR interferometer.

Figure 2 (a) shows the time history of the line-integrated density increase $\Delta(n_e l) \equiv (n_e l)(t) - (n_e l)(t = 0)$ during the neon pellet injection for discharge 158161. Here we take $t = 0$ ms at the beginning of ablation emission. The pellet injection velocity and the target core electron temperature were 559 m/s and 1.91 keV, respectively. Figure 2 (a) shows that although there is a slight density increase about $\Delta(n_e l) \lesssim 1 \times 10^{19}$ m^{-2} in early phase, the significant electron density rise occurs after 0.6 ms and peaks up to 20×10^{19} m^{-2} at 1 ms after the ablation emission starts. Figure 2 shows the same plot for deuterium injection into the almost identical condition, where the injection velocity is $V_p = 569$ m/s and $T_{e0} = 1.92$ keV. The behavior of the $\Delta(n_e l)$ signal for the neon injection is qualitatively similar between the two cases but the response of $\Delta(n_e l)$ looks much slower for the neon injection than in the case of deuterium injection. Such a relatively slow response of the density signals as compared to the hydrogen isotope pellets was observed commonly between all the 8-pellet data for neon injection.

3. Comparison to Pellet Ablation Code

3.1 NGPS ablation code

For interpreting the observation, we applied the numerical pellet ablation code based on the neutral gas and plasma shielding (NGPS) model [5] (which is referred to as the NGPS code below). For the present study, we have adapted the NGPS model of [6] to neon species through the

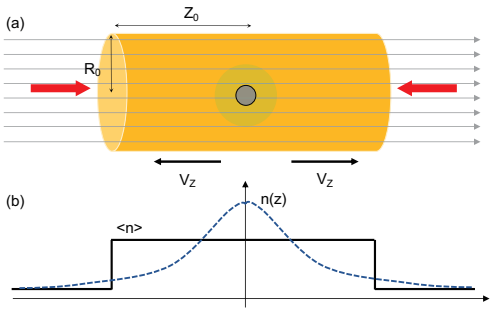

Fig. 3 (a) A model of the ablation cloud assumed in the NGPS code. (b) The density profile along the field line is not considered but is approximated by uniform plasma parameters inside the ablation cloud.

implementation of the physical properties (gas properties, ionization, recombination, and radiation) and the collision cross section data. While the physical assumption applied in the NGPS model has been described in [6], more detailed description of this extended version will be reported elsewhere.

Figure 3 (a) shows a model of the ablation cloud assumed in the NGPS code. One feature of this code is to evaluate the expansion of ionized cloud outside the neutral cloud surrounding the pellet. Because the external magnetic field stops the perpendicular expansion of the ionized cloud, the ablation cloud expands preferentially along the magnetic field at the sound velocity. For simplifying the problem, the model of [5] assumed that the density profile along the magnetic field is described by a single value in terms of the volume-averaged density, as schematically illustrated in Fig. 3 (b).

Another feature of our NGPS code is to evaluate not only the ablation by thermal electrons but by fast ions. This model was applied to the analysis of hydrogen pellet injection on the LHD [5], showing that the beam energy of tangential NBI system on the LHD is high enough to have significant contribution and it is essential to take into account it for reproducing the measured penetration depths. In the experimental data analyzed here, the hydrogen beams were injected into both hydrogen and deuterium discharges. The ablation rate due to fast hydrogen has been evaluated using the NGPS model of [6] with the hydrogen stopping power on neon. Because tangential NBI system in the LHD is based on negative-ion beam sources, slowing down distribution with single beam component of 180 keV gives reasonable approximation of the energy and pitch-angle distribution of hydrogen beam ions. Below we find that the contribution of fast ions is also not negligible for the ablation of neon pellets in the LHD.

3.2 Electron density response

Figures 4 and 5 illustrate the time history of the cloud parameters calculated by the NGPS code. The plasma and pellet parameters were based on the experimental data of

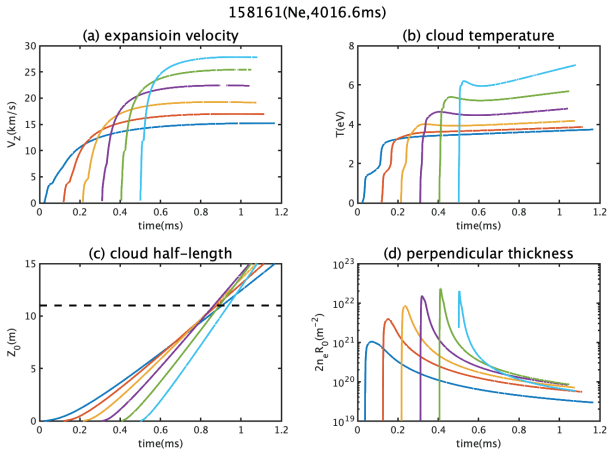

Fig. 4 (a) Plasmoid expansion velocity; (b) temperature; (c) cloud half-length; (d) line-integrated density calculated by the NGPS code for the neon injection of #158161.

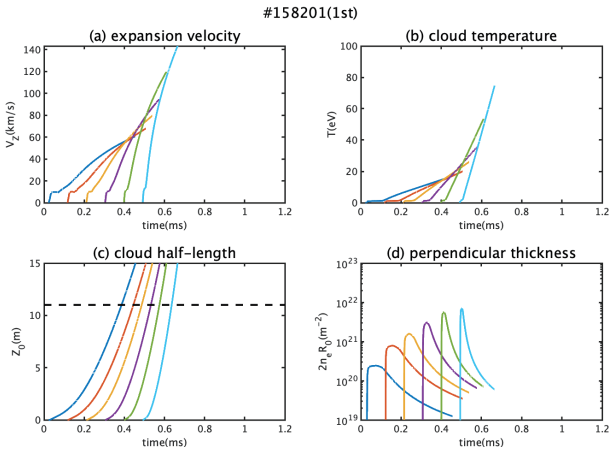

Fig. 5 The same figure with Fig. 4 for the deuterium pellet injection of #158201.

the two shots in Fig. 2. Each curve corresponds to the calculation for the ablation cloud released at the first six points along the pellet path of Fig. 1 (b). Hence the one released at the later time is exposed to hotter plasma and is therefore heated more efficiently than those released at the plasma periphery in earlier time. Within such a variation, expansion velocities of the neon cloud are seen to increase up to 15 - 28 km/s. The expected timescale required for the ablated materials to reach the density measurement location, which is 11 m far from the ablation position, is evaluated to be 0.87 - 0.94 ms. Because the expansion velocity of the ablation cloud is close to the sound velocity $\propto (\gamma T/m)^{1/2}$ (where γ is the specific ratio of heat and m is the pellet atomic mass), a relatively slow assimilation occurs for neon owing to that the cloud temperature remains 3.6 - 6.9 eV until the ablation cloud expands up to 15 m. Such a low temperature is due to that strong line emission inside dense neon clouds plays a role in the electron energy loss. In contrast, the NGPS code has shown that because

the energy loss associated with line emission is not significant, the ablation cloud of the deuterium pellet is immediately heated up to tens of eV. High temperature ablation cloud leads to quick expansion of the ablated materials up to 68 - 142 km/s along the magnetic field line. The estimate for the expansion time up to $Z_0 = 11$ m is 0.38 - 0.63 ms. In Fig. 2, the expansion timescales for neon and deuterium injection have been displayed using the filled intervals. The relative delay of the $\Delta(n_e l)$ signals for neon as compared to hydrogen ones is consistent with the expansion timescale estimated by the NGPS code. Concerning the magnitude of density increase, the calculated perpendicular thickness $2n_e R_0$ of the cloud around 10^{20} - 10^{21} m^{-2} is in reasonable agreement with the observed line-integrated density increases about $15 - 20 \times 10^{19}$ m^{-2}. This is unexpectedly good agreement although the NGPS code neglects the density profile of the plasmoid [see Fig. 3 (b)]. In fact, the NGPS code did not capture the timing of the $\Delta(n_e l)$ peak in time consistently between neon and hydrogen pellets in Fig. 2. To reproduce the observations in such levels, more complex simulations that account for three-dimensional structure of the plasmoid in realistic magnetic-field geometry would be necessary.

3.3 Neon pellet penetration depth

Because the pellet ablation model used by SPI simulations has been based on the neutral gas shielding (NGS) model [7], its validation is essentially important for the prediction of the ITER DMS performance. If one assumes linear profiles for the electron temperature and density along the pellet penetration depth λ [8], we can derive the penetration depth scaling to have a form given by

$$\frac{\lambda}{a} = C T_{e0}(\mathrm{keV})^{-5/9} n_{e0}(10^{20}\mathrm{m}^{-3})^{-1/9} \times N_p(10^{20}\mathrm{atoms})^{5/27} V_p(\mathrm{m/s})^{1/3}, \quad (1)$$

where a, T_{e0}, n_{e0}, N_p, and V_p are the plasma minor radius, the central electron temperatures and densities, the pellet particle content, and the pellet velocity. The numerical factor C is calculated to be 0.080 for hydrogen isotope using the NGS model. The same approach to neon using the physical constants of [9] leads to $C = 0.1894$. In the present experiments, the linear profile assumption in Eq. (1) can reasonably approximate the observed T_e profile without steep edge pedestals.

Red curves of Fig. 6 show the mapping of ablation emission on the major radius R by assuming that the pellet keeps the constant velocity during its penetration. For the comparison, we have omitted 2 of 8 discharges because these two pellets passed the plasma centre and so-called self-limiting effect [10] makes the comparison with the models not straightforward. The remaining 6 shots include the data with the central electron temperature and density of the target plasmas in the range between 1.1 keV $\lesssim T_{e0} \lesssim$ 1.9 keV and $3.0 \lesssim n_{e0} \lesssim 7.5 \times 10^{19}$ m^{-3}, respectively. The emission increases as the pellet penetrates into

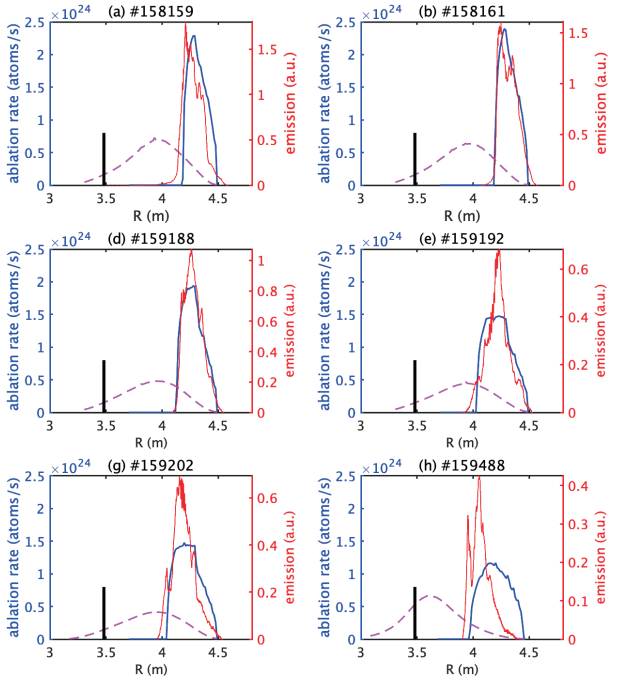

Fig. 6 Mapping of the ablation emission for the 6-pellet data (red). Black lines are the expected penetration depths from the NGS scaling law. Solid blue and dashed magenta curves are the calculated ablation profiles using the NGPS ablation code [5] with and without the contribution of fast ions, respectively.

hotter plasma in the direction of decreasing R and stops at the end of evaporation. The black line in each figure represents the penetration depths estimated by Eq. (1) and we see that the measured penetration depths are shallower than the NGS scaling by up to a factor of 2.

The above discrepancy between the measured penetration depth and the NGS scaling can be resolved by the NGPS code. In Fig. 6, two calculations (solid blue and dashed magenta curves) are presented to compare the ablation profile with and without the contribution of fast ions, showing the reasonable agreement with the measured penetration depth when the fast-ion ablation is included. These code predictions given by the blue curves have well reproduced the measured penetration depths within 10 cm. This suggests that as in the case of hydrogen pellets previously studied [5], the fast ions play a dominant role in the ablation of neon pellets in the LHD.

4. Summary

Motivated by the contribution to ITER DMS physics validation, we have performed the neon pellet injection experiment on the LHD. The post-injection density measurement by the FIR interferometer has pointed out a relatively slow assimilation of the ablated materials as compared to the case of hydrogen isotope pellet injection. The analysis using the NGPS ablation code has shown that strong line emission inside the ablation cloud limits the cloud temper-

ature and the expansion velocity of ablation clouds.

The measured penetration depths were also compared, showing that the NGPS ablation code well reproduces the measured penetration when the code takes into account the contribution from 180 keV beam ions. The latter point may raise a question whether ITER 1 MeV NBI affects the ablation and assimilation properties of ITER DMS pellet material, which is a subject of the future work.

Acknowledgement

The authors gratefully acknowledge the support from the LHD experiment group. This work was supported by NIFS20ULPP004 and in part by Grants-in-Aid for Scientific Research (MEXT KAKENHI Grant No. 21H01070) and was partially performed under the auspices of the ITER Scientist Fellow Network.

[1] M. Lehnen *et al.*, Proceedings for the 27th IAEA Fusion Energy Conference (Gandhinagar, Oct 22-27 2018) [EX/P7-12].
[2] T.E. Gebhart, L.R. Baylor and S.J. Meitner, IEEE Trans. Plasma Sci. **48**, 1598 (2020).
[3] R. Sakamoto *et al.*, Rev. Sci. Instrum. **84**, 083504 (2013).
[4] S.L. Milora and C.A. Foster, Rev. Sci. Instrum. **50**, 482 (1979).
[5] A. Matsuyama *et al.*, Plasma Phys. Control. Fusion **54**, 035007 (2012).
[6] B. Pégourié *et al.*, Plasma Phys. Control. Fusion **47**, 17 (2005).
[7] P.B. Parks and R.J. Turnbull, Phys. Fluids **21**, 1735 (1978).
[8] L.R. Baylor *et al.*, Nucl. Fusion **37**, 127 (1997).
[9] B.V. Kuteev, V. Yu. Sergeev and S. Sudo, Nucl. Fusion **35**, 1167 (1995).
[10] S.L. Milora *et al.*, Nucl. Fusion **20**, 1491 (1980).